Received: 21 April 2021 | Revised: 5 July 2021 | Accepted: 20 July 2021

DOI: 10.1002/ar.24766

AR WOW - VIDEO ARTICLE

The Anatomical Record

WILEY

Anuran development: A reinvestigation of the conus arteriosus and gill formation in *Bufo bufo* throughout metamorphosis using micro-CT

Nina Kraus | **Brian Metscher**

Department of Evolutionary Biology Theoretical Biology Unit, University of Vienna, Vienna, Austria

Correspondence
Brian Metscher, Department of Evolutionary Biology Theoretical Biology Unit, University of Vienna, Vienna, Austria.
Email: brian.metscher@univie.ac.at

Abstract

Using high-resolution X-ray micro-CT imaging of whole *Bufo bufo* specimens, we acquired detailed 3D descriptions of the changing morphology of the cardiac outflow structures, in particular the conus arteriosus through larval development and the transition. Previous findings regarding anuran conal structures were contradictory, depending on the specifics of the 2D imaging methods used by different authors. Our descriptions of conal morphology at different developmental stages show that early tadpoles initially only have one opening at the ventricular-conal junction and only one cavum within their conus; however, the forming septum coni soon divides the conus into two chambers, the cavum pulmocutaneum and the cavum aorticum. This is accompanied by the development of a second small opening at the ventricular-conal junction. The separated chambers continue into the aortic arches. Following the aortic arches into the area where gills will form, we describe how blood vessels associated with the external gills develop from vessels arising from the truncus arteriosus. The external gills soon undergo partial absorption. During the transition from external to internal gills, the gill filaments retreat asymmetrically into a gill chamber formed by a hyoidal cover contacting the animal's ventral side, leaving only a single opening on the animal's left side, the opercular spout. *B. bufo* retains its internal gills up to metamorphic climax, with the aortic arches arising from the conus arteriosus still leading into the gills. Our 3D image data are publicly available and will provide a sound morphological basis for future studies.

This article includes AR WOW Videos, which can be viewed at Video 1: https://players.brightcove.net/656326989001/default_default/index.html?videoId=6272314129001; Video 2: https://players.brightcove.net/656326989001/default_default/index.html?videoId=6272314969001; Video 3: https://players.brightcove.net/656326989001/default_default/index.html?videoId=6272315263001; Video 4: https://players.brightcove.net/656326989001/default_default/index.html?videoId=6272314128001; Video 5: https://players.brightcove.net/656326989001/default_default/index.html?videoId=6272313712001.

KEYWORDS

3D imaging, amphibian, *Bufo*, cardiac embryology, conus arteriosus, development, vertebrates, X-ray microtomography

1 | INTRODUCTION

During early embryonic development of anurans, two mesodermal heart anlagen fuse to form a linear heart tube that then twists during cardiac looping and later gives rise to the distinct chambers of the adult heart (Mohun, Leong, Weninger, & Sparrow, 2000). Once this compartmentalization is finished, the anuran heart consists of a sinus venosus leading into an atrium with a complete atrial septum, which connects to a ventricle with muscular trabeculae but no septation (Kardong, 2009). (The sinus venosus is arguably not a true heart chamber because it does not form by ballooning; Jensen et al., 2013.) Absence of a septate ventricle is a unique condition within true lung-breathing vertebrates (Johansen & Hanson, 1968). This ventricle further leads into the outflow tract, which consists of a muscular conus arteriosus with two rows of valves and a septum (often called either the spiral valve or septum coni) as well as the truncus arteriosus (see Figure 1).

The general morphology of the conus arteriosus is not agreed upon. Comparisons of published descriptions of the conus arteriosus reveal important contradictions regarding the morphology of the valves within it, and regarding the spiraling pattern of the septum coni and its anterior attachment to the wall of the conus arteriosus (Ison, 1967, 1968; Sharma, 1961; Simons, 1957). Note that, here, valves refers to the individual leaflets or cusps around an orifice, while in human anatomy, a valve usually refers to the whole structure around an orifice that consist of a number of valve leaflets or cusps.

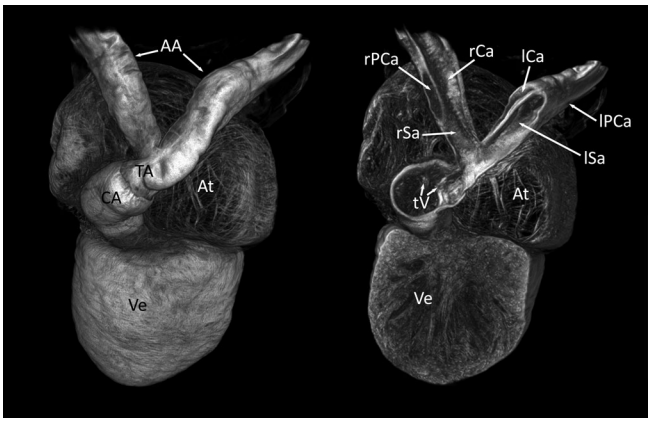

FIGURE 1 Volume rendering (left) and virtual cutaway (right) of a PTA-stained whole adult heart of *Bufo bufo*. AA, aortic arches; At, atrium; CA, conus arteriosus; lCa, left carotid arch; lPa, left pulmocutaneus arch; lSa, left systemic arch; rCa, right carotid arch; rPCa, right pulmocutaneus arch; rSa, right systemic arch; TA, truncus arteriosus; tV, top valves; Ve, ventricle. Video 1 (cutaway_whole_heart_Bufo) shows a virtual cutaway of the same specimen. Video 2 (Bufo_conus_cutaway_sloweddown) shows a virtual cutaway of just the conus in more detail

The number of valves reported within the conus arteriosus varies dramatically depending on whether the authors sectioned their samples horizontally or transversely, as pointed out by Ison (1967). By producing and analyzing both transversal and horizontal histological sections, Ison was able to obtain a much more three-dimensional picture of conus morphology for adult *Rana temporaria*.

Following conus morphology throughout development is necessary to better understand anuran hearts. Ison (1968) addressed this as well, but labor- and time-intensive reconstruction from histological sectioning limited the 3D results for the extremely rapidly developing anuran heart.

Other than Ison's work, most developmental studies focused on very early heart development (Mercola, Guzzo, & Foley, 2010), stopping shortly before the main parts of the heart are fully differentiated, or the work was simply not focused on conus morphology (Kolker, Tajchman, & Weeks, 2000). A developmental study by Mohun et al. (2000) on *Xenopus laevis* did mention the appearance of valves and the septum coni, but the authors also mention that the 3D methods used were not adequate to trace later events of valve formation and conus septation. They again relied on histological sections which were then reconstructed in 3D. However, this method tends to have difficulties with aligning sections, which can be especially important with small, intricate structures such as the conus structures.

Additionally, the morphological basis for the metamorphic transition from external to internal gills tadpoles undergo awaits detailed description. A thorough literature search turned up only a short note by Rugh (1951) saying that the hyoid arch goes on to form parts of the tadpole's operculum.

To fill these gaps in the literature and to resolve the morphology of the conus arteriosus of a representative species, *Bufo bufo*, we used 3D X-ray microtomography imaging (micro-CT) to analyze the structure of the anuran conus arteriosus throughout metamorphosis in order to establish a strong foundation on which to base future research on the anuran cardiovascular system. We also describe the development of the gross heart morphology, which has not been previously done for *B. bufo*. Moreover, we describe gill morphology during development to contribute to the

understanding of the transition between the different modes of respiration in larval anurans. Our 3D image data are publicly available and can be used as a basis for future research on the heart and gill morphology of *B. bufo*.

2 | METHODS

2.1 | Samples

Specimens of *B. bufo* were acquired from the herpetological collection of the Natural History Museum of Vienna. Samples were previously fixed and stored in a solution of 50% EtOH and 5% formalin. Using a stereomicroscope, developmental stage was assigned according to the Gosner staging table (Gosner, 1960), which is based on external morphological characteristics of anuran larvae. A list of the specimens is included with the archived 3D image data at Zenodo.org.

2.2 | Staining

Specimens younger than Gosner stage 43 were stained using 0.3% PTA in 70% EtOH (Metscher, 2009). First, those specimens were washed in 70% EtOH three times, for about 15 min each. Then, those specimens were transferred to the staining solution for 24–48 hr, depending on size. Subsequently, the specimens were washed again in 70% EtOH for at least 1 hr with one change to fresh 70% EtOH during this period.

Due to the increased thickness of the epidermis in older specimens, starting from Gosner stage 43, aqueous iodine (Lugol's solution, IKI; Metscher, 2009) was used as a contrast stain. These specimens were initially rehydrated by a descending alcohol series (50% and 30% EtOH for 30–60 min each). Later, those specimens were washed in distilled water twice for at least 15 min each. After rehydration, the specimens were moved to IKI solution for about 48 hr and after that were again washed in distilled water twice, for about 30 min each.

Additionally, a single specimen was stained with Rose Bengal (an iodated eosin analog; Chroma 1A 182) at 0.5% in 50% EtOH, and after micro-CT scanning, it was embedded in paraffin and sectioned at 7 μm. The slides were dewaxed in two washes of xylene (5 min each) and then cover slipped without further staining because additional staining and processing would have risked further dehydration of the cardiac jelly, making it harder to see.

2.3 | Micro-CT imaging

After staining, intact specimens were mounted in 1% aqueous agarose (Metscher, 2011) for scanning. Specimens were scanned using a Xradia MicroXCT microtomography imaging system (Zeiss X-Ray Microscopy) with a tungsten X-ray source operated at 40 to 60 kV and 4 W. Individual projection images were taken every 0.20° over a 180° scan, with 40 s exposure times. The tomographic sections were reconstructed with voxel sizes of 0.89 to 3.99 μm using the XMReconstructor software supplied with the system.

The complete reconstructed tomographic images are available as TIFF stacks on the Zenodo repository (doi: 10.5281/zenodo.5052677).

2.4 | Analysis

Scans were conducted starting from Gosner stage 18, but the main focus was on scans starting from Gosner stage 19 (the time the heart starts to beat) up to stage 46 (a small froglet that has just finished metamorphosis). Earlier development was excluded from this study, since it has already been covered extensively by other authors (Mohun et al., 2000; Rugh, 1951).

Initially, one specimen was scanned per developmental stage. If initial analysis showed that developmental changes are too rapid to be fully covered by the Gosner table, which is only based on external morphological

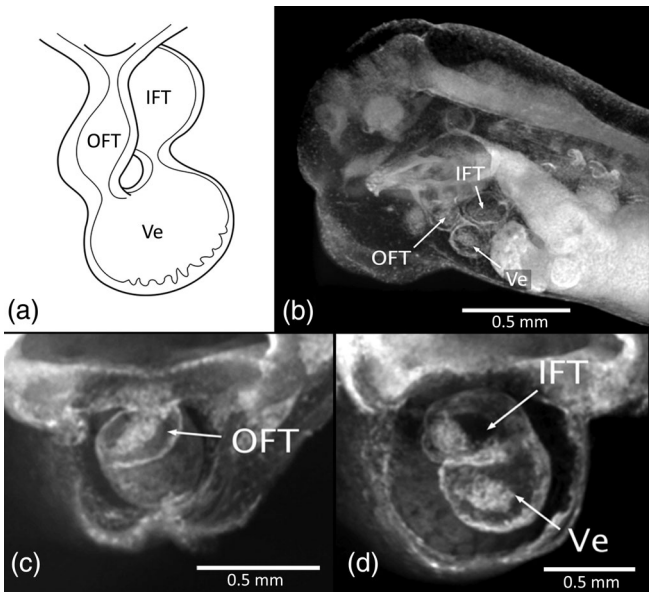

FIGURE 2 *Bufo bufo* heart morphology at Gosner 19. (a) Schematic drawing of the gross heart morphology at this developmental stage, ventral view. (b) Volume rendering of a contrast-enhanced micro-CT image, virtual parasagittal cutaway showing a lateral overview. (c) Rostral view of a virtual transversal cutaway. (d) Rostral view of a virtual transversal cutaway, more posterior than (c). IFT, inflow tract; OFT, outflow tract; Ve, ventricle

characteristic, more scans were conducted of the specific developmental stage.

Obtained images of specimens were examined and described using the Xradia XM3DViewer software, Dragonfly 3.6 (http://www.theobjects.com/dragonfly) and Amira 6.4 or 2020.2 (ThermoFisher Scientific). Segmentations were made using the Dragonfly 3.6 segmentation tool. Images and segmentation where additionally compiled and used for making schematic drawings of the overall heart morphology, as well as conus morphology. Those drawing were digitized using Inkscape (http://www.inkscape.org/). General image manipulation and labeling were done with Fiji (Schindelin et al., 2012) and its plugin FigureJ (Mutterer & Zinck, 2013), or with Adobe Photoshop.

3 | RESULTS

3.1 | Tadpole heart and outflow tract development

At Gosner stage 18, the two endocardial tubes are already fully fused, the heart has already started to coil into its distinct spiral- or S-shape, and the main components of the heart can already be distinguished.

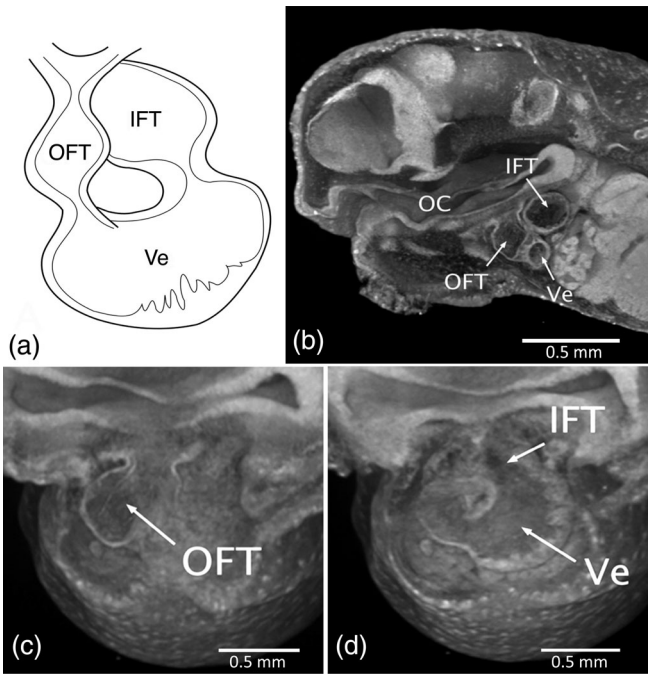

FIGURE 3 *Bufo bufo* heart morphology at Gosner 21. (a) Schematic drawing of the gross heart morphology at this developmental stage, ventral view. (b) Micro-CT volume rendering, lateral overview of a virtual parasagittal cutaway. (c) Rostral view of a virtual transversal cutaway. (d) Rostral view of a virtual transversal cutaway, more posterior than (c). IFT, inflow tract; OC, oral cavity; OFT, outflow tract; SC, septum coni; Ve, ventricle

At Gosner stage 19 (Figure 2), the heart tube's inflow area (future atria) is still connected to the yolk via the vitelline veins. With the whole heart coming to lie in the

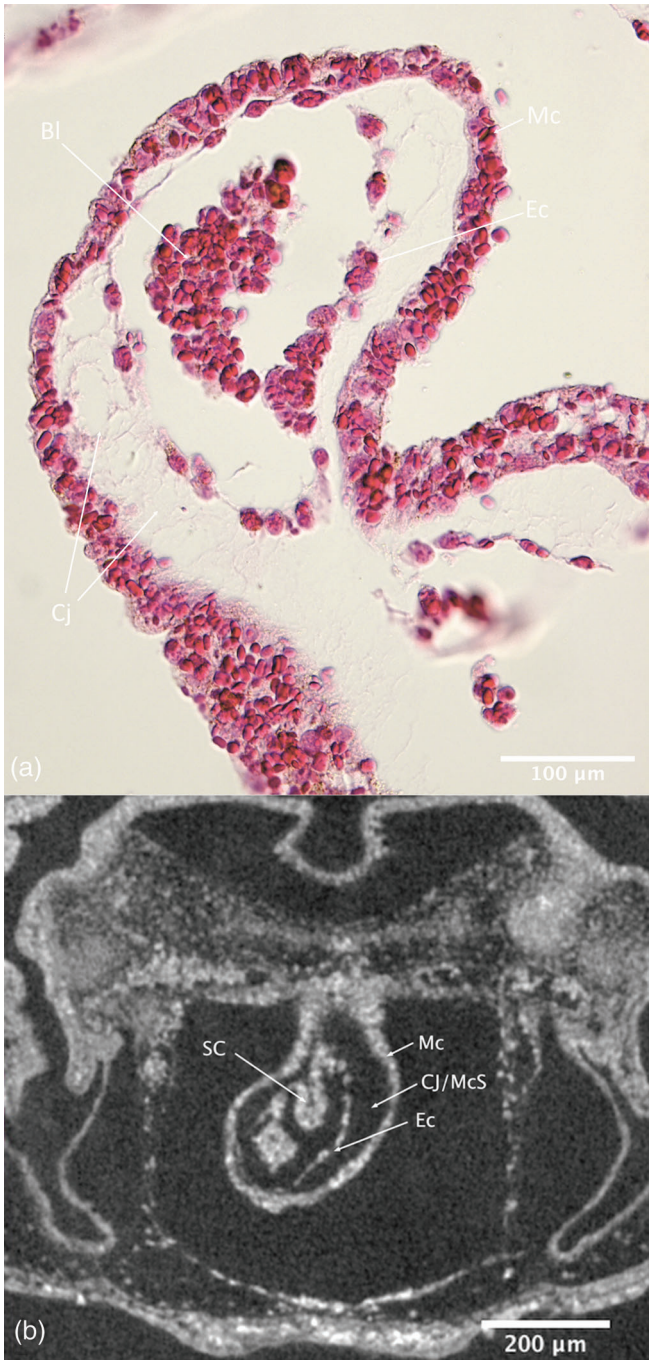

FIGURE 4 The typical three-layered structure of an embryonic vertebrate heart with the myocardium on the outside and endocardium on the inside of the heart with the cardiac jelly in between. (a) Horizontal histological section through a Rose Bengal-stained conus arteriosus of a *Bufo bufo* tadpole at Gosner stage 22. (b) Micro-CT image of the same specimen: virtual section through the transversal plane showing the conus arteriosus (more ventral than a) and the formation of the septum coni. Bl, blood cells; Cj, cardiac jelly; CJ/McS, cardiac jelly/myoendocardial space; Ec, endocardium; Mc, myocardium

animal's center line the inflow area is bent to the right and lies dorsally under the mouth opening. The heart tube then bends ventrally and to the left, leading into the ventricle. The ventricle itself already started to balloon at this point, taking on a wide U-shape, with its most dorsal curvature being concave. Subsequently, the heart tube twists dorsally and to the right, leading into the outflow area (the future conus).

At this point in development, the formation of trabeculae within the ventricle begins, starting from the structures middle, the apex, and proceeding toward the inflow and the outflow area. In those areas themselves, however, the embryonic heart tissues have not yet started to differentiate morphologically, so the typical three-layered

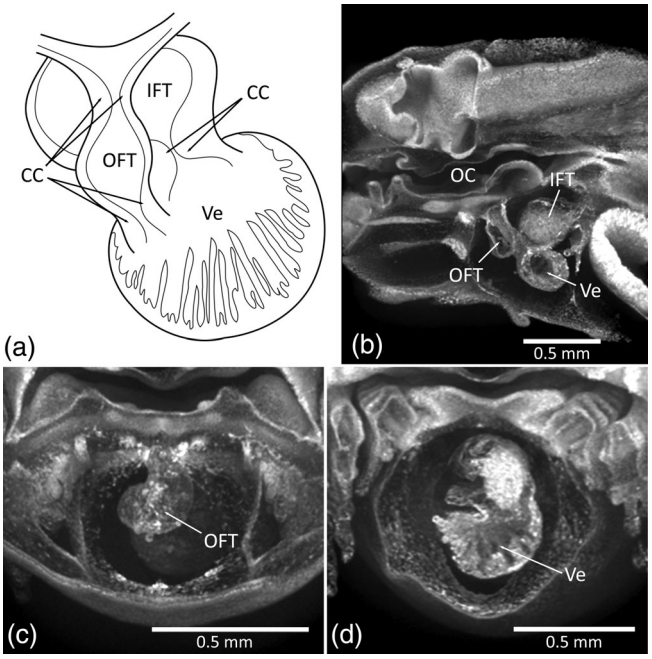

FIGURE 5 *Bufo bufo* heart morphology at Gosner 23. (a) Schematic drawing of the gross heart morphology at this developmental stage, ventral view. (b) Micro-CT volume rendering, lateral overview of a virtual sagittal cutaway. (c) Rostral view of a virtual transversal cutaway. (d) Rostral view of a virtual transversal cutaway, more posterior than (c). CC, cardiac cushions; IFT, inflow tract; OC, oral cavity; OFT, outflow tract; Ve, ventricle

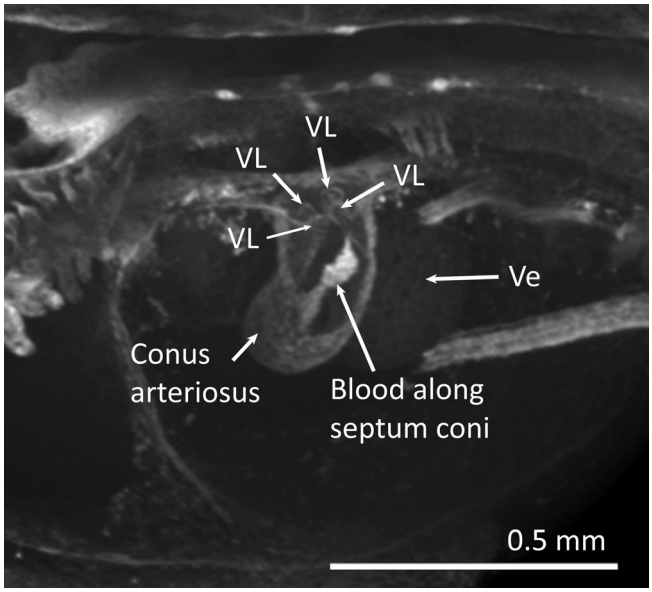

FIGURE 7 Virtual cutaway through the transverse plane of a 3D reconstruction of a *Bufo bufo* tadpole at Gosner stage 24 showing the now-distinct four leaflets of the two top valves. As in Figure 6, the septum coni is obscured in this volume rendering by blood fixed along it. Ve, ventricle; VL, valve leaflets

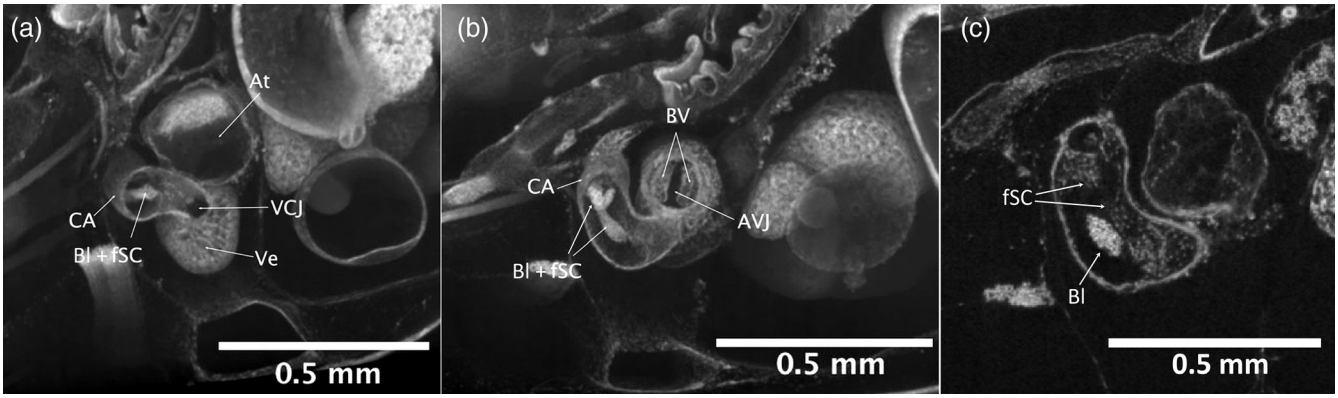

FIGURE 6 Virtual cutaways and virtual section of a 3D rendering of a *Bufo bufo* tadpole at Gosner stage 24 showing how the atrium mouths into the ventricle at the atrio-ventricular junction and the bicuspid valves of the atrium, and where the conus mouths into the ventricle at the ventricular-conal junction, as well as the spiraling pattern of the conus and the septum coni. In the volume rendering, the forming septum coni is obscured by fixed blood, which stains more strongly with PTA; this can be seen clearly in the section. (a) Virtual cutaway in sagittal plane. (b) Virtual cutaway in transverse plane. (c) Virtual section in an oblique plane. At, atrium; AVJ, atrio-ventricular junction; Bl, blood; BV, bicuspid valves; CA, conus arteriosus; fSC, forming septum coni; VCJ, ventricular-conal junction; Ve, ventricle

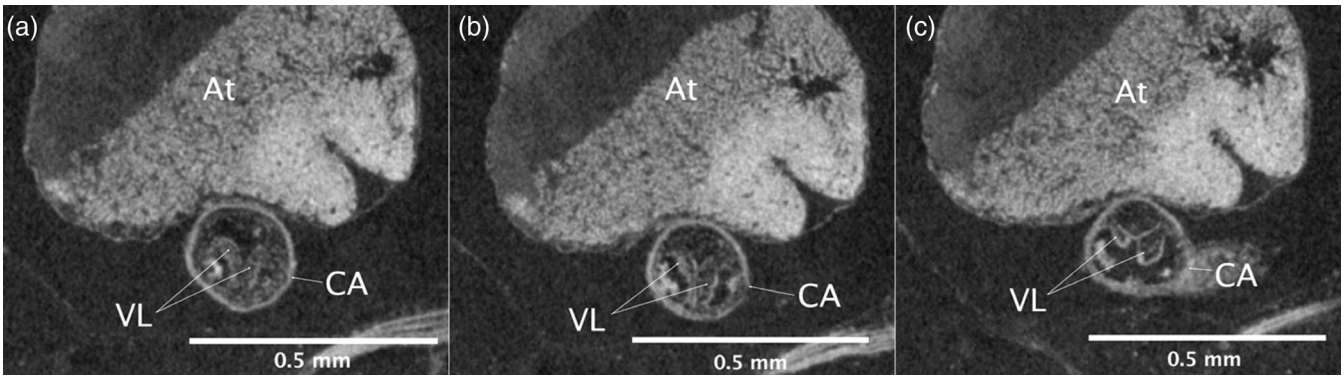

FIGURE 8 Virtual sections through the frontal plane of the conus arteriosus of a *Bufo bufo* tadpole at Gosner stage 29 showing the leaflets of the top valves contacting each other to form the distinctive Y-shape, (a) being the most caudal one, (b) the most rostral one. At, atrium; CA, conus arteriosus; VL, valve leaflets

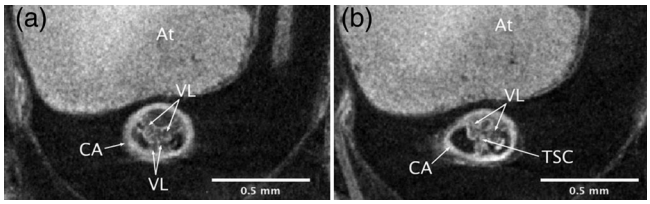

FIGURE 9 Virtual sections through the frontal plane of the conus arteriosus of a *Bufo bufo* tadpole at Gosner stage 36 showing the leaflets of the top valves contacting each other to form the distinctive Y-shape. Note that (a) the more dorsal valve leaflets closing off the entry of the cavum pulmocutaneum into the pulmocutaneus aortic arch reach further rostral (b) than the ones closing off the cavum aorticum and reaching into the systemic and carotid aortic arches. At, atrium; CA, conus arteriosus; TSC, tip of septum coni; VL, valve leaflets

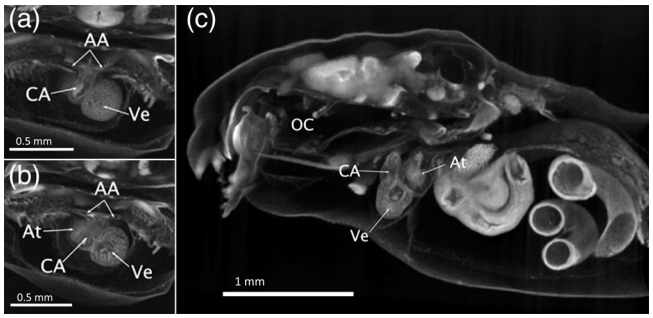

FIGURE 10 *Bufo bufo* heart morphology at Gosner 25. (a) Rostral view of a virtual transversal cutaway. (b) Rostral view of a virtual transversal cutaway, more posterior than (a). (c) Lateral overview of a virtual parasagittal cutaway. AA, aortic arches; At, atrium; CA, conus arteriosus; OC, oral cavity; Ve, ventricle

structure of the embryonic vertebrate heart is still fully present (see Figure 4).

Little changes up to Gosner stage 21, when the rate of heart development starts to increase. Hence, developmental changes are too rapid to be fully covered by the Gosner table, so several scans were made of specimens within this stage.

During stage 21 (Figure 3), the inflow area/atrium starts to balloon and increases in diameter. The ventricle continues to balloon as well, and thereby becomes rounder and less U-shaped than previously, meaning the initially concave top curvature becomes more convex. Trabeculation proceeds toward outflow and inflow area, so that the full width of the ventricle is in the process of becoming trabeculated. Already existing trabecula become more pronounced. At the top curvature are no trabeculae, so cardiac jelly remains. The outflow area becomes more elongated and tilts more ventrally and less to the right than prior. Its layer of cardiac jelly becomes thinner.

With stage 22, the S-shaped coiling of the heart tube becomes tighter, so the distances between outflow area, ventricle and inflow area become smaller and the outflow area comes to lie in front of the inflow area (see Figure 5 for relation of those structures to each other). The ventricle is already very round and appears fully trabeculated.

Starting at Gosner stage 22, the atrial septum starts to appear. Also, cells of the endocardial layer within the conus start to migrate into its cardiac jelly. This leads to a small, tongue-shaped structure that protrudes from the right dorsal side of the conus, reaching downward and curving in the same fashion as the conus itself does (Figures 4b and 6). This protrusion will go on to form the septum coni. It initially contacts a ring of tissue at the junction of the conus arteriosus and the ventricle, but at a later phase of this Gosner stage, only its tip still contacts the valves and the septum coni elongates. At this point however, there is only a single cavum within the conus, through which blood could potentially flow.

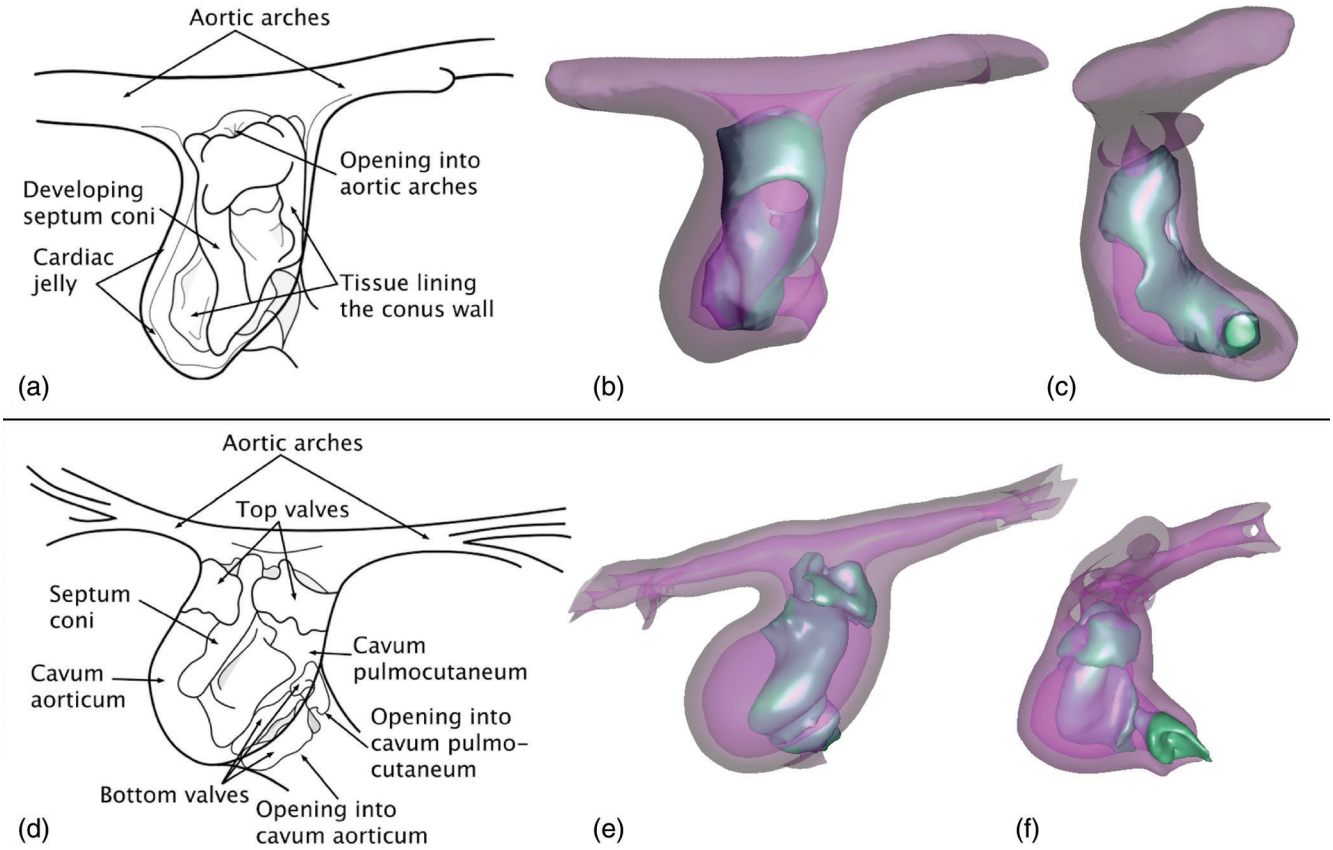

FIGURE 11 Schematic drawings of the conus arteriosus morphology (ventral view) of *Bufo bufo* and segmentations at the respective stages (pink: conus wall, green: conal structures) through anuran heart development. (a) Conus arteriosus at Gosner stage 22. Here, the septum coni does not yet lie close to rostral wall of the conus, so instead of dividing it into two chambers, it allows for blood flow in front of it. At this point in development, the conus shows no distinct valves and is still mostly lined by a thin sheet of tissue. (b) Segmentation of a Gosner stage 22 specimen in rostral view. (c) Segmentation of a Gosner stage 22 specimen in lateral view. (d) Conus arteriosus at Gosner stage 43: the septum coni has already grown significantly toward the rostral conus wall but is not in direct contact with it. The two main bottom walls and the small extra valve or leaflet are already fully formed, allowing for two separate entries for blood into the conus. The morphology suggests that blood entering via the small opening at the ventricular-conal junction will flow into the cavum pulmocutaneum, while blood entering via the main opening leads into the cavum aorticum. The two cava are separated via the septum coni. (e) Segmentation of a Gosner stage 43 specimen in rostral view. (f) Segmentation of a Gosner stage 43 specimen in lateral view. Videos 3 (stage_22_contour_mesh_conus) and 4 (stage_43_contour_mesh_conus) show the rotating segmentations of the conus at stage 22 and 43, respectively

The ring of tissue at the bottom of the conus as well as on its top starts to form from endocardial cushions that start to appear at Gosner stage 23 (Figure 5). The bottom ring of tissue develops a small protrusion within Gosner stage 23 that contacts the septum coni. The septum coni itself starts to grow thicker and to become more prominent and is clearly cellularized (see Figure 6c). At this stage as well, a small extra opening from the ventricle into the conus starts to appear in this ring of tissue. It lies more caudally than the main opening and remains rather small and narrow (see Figures 11d–f and 17).

From Gosner stage 24 to 25, the endocardial cushions at the top (Figure 7) and bottom (Figure 17) of the conus develop into defined valves which at this point are all connected to other structures within the conus via a thin lining of a sheet of tissue (as is shown in Figure 11a–c). Once the bottom valves are more defined, it is visible that the septum coni contacts the smallest of those valves (the left one), which lies closest to the atrial opening of the ventricle. Additionally, those valves are connected to the septum coni not only by this protrusion, but also by a lining of tissue of the right side of the conus. On the left side, this lining is significantly thinner. While there seemed to be minor individual differences, this bottom ring of valves consists of two main valves and a small extra protrusion that contacts the septum coni, which can be understood as its own small valve (see Figure 17). At the top, there are two main valves, each made up of two leaflets, but again, they form a continuous ring of tissue that is connected to the conus wall (see Figure 7).

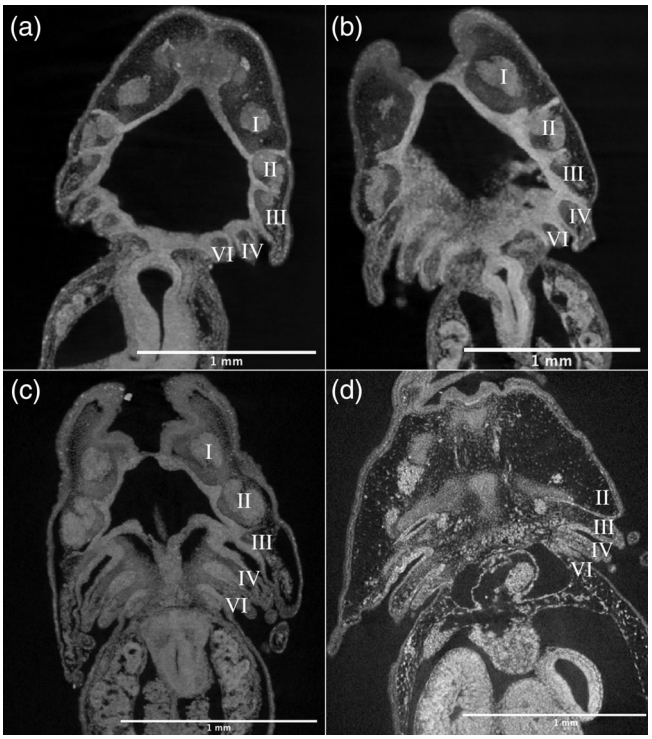

FIGURE 12 Overview of the development of the pharyngeal arches in virtual thick sections through the horizontal plane of *Bufo bufo* tadpoles at different developmental stages. (a) Late Gosner stage 18. (b) Gosner stage 19. (c) Gosner stage 21. (d) Gosner stage 23. I: mandibular arch; II: hyoid arch; III: third arch; IV: fourth arch; VI: sixth arch; Vth arch is not present in anurans

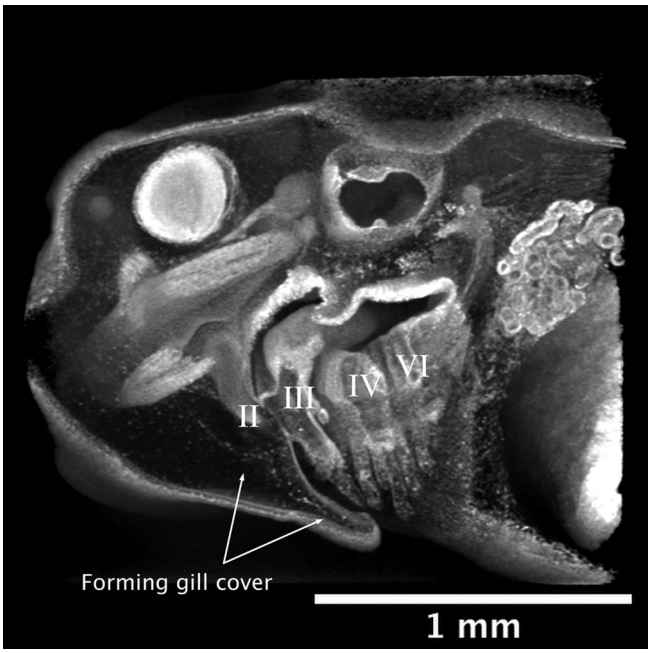

FIGURE 13 Virtual parasagittal cutaway of a *Bufo bufo* tadpole at Gosner stage 23 in lateral view showing the gill cover forming. II: hyoid arch; III: third arch; IV: fourth arch; and VI: sixth arch

At this point in heart development, the septum coni grows an additional small protrusion that grows upward and reaches into the middle of the top row of valves (see Figures 9, 11d–f, and 16). This leads to those structures forming a "Y" that divides three small chambers within the junction of the conus into the aortic arches (see Figures 8, 9, 11d–f, and 16). The dorsal one of those is connected to the pulmocutaneous arch, while the other two, more ventrally lying cava are connected to the systemic and the carotid arches. The reduction of the conus lining and the connection of the tongue-shaped septum coni to the bottom valves, as well as the appearance of the small extra opening at the base of the conus results in two cava within the conus, through which blood could potentially flow. Additionally, the small protrusion on one of the bottom valves of the conus has lost direct contact to the conus wall, creating a very small, additional way blood could potentially enter the conus from the ventricle. Since this protrusion is connected to the septum coni, this opening aligns with the left cavum of the conus, the cavum pulmocutaneum, while the large opening formed by the ring of valves aligns with the right cavum, the cavum aorticum. The right cavum connects to the openings of the two valves into the systemic and carotid arches, and the cavum on the left side connects to the opening to the pulmocutaneous arches. From this point on, there are two cava within the conus that continue throughout the whole length of the conus and its junction into the aortic arches.

After Gosner stage 25 (Figure 10), conus development starts to slow down again. However, the thin sheets of tissue lining the conus walls, which connected top and bottom walls, as well as septum coni, grow thinner. Since this lining has already been thinner on the left side of the conus, it vanishes sooner than the lining on the right. This slow reduction of this conus wall lining continues up to Gosner stage 28, leaving only the tip of the septum coni in contacts with small bottom valve at the left, with all other structures within the conus looking like distinct units by now (see Figure 11d–f). In addition, the valves and the septum coni grow thinner, leading to the general heart morphology to look more delicate. At this point, the scans show fewer nuclei in these structures.

After Gosner stage 30, there are no further changes to either the overall heart morphology or the structures within the conus arteriosus. But the heart continues to grow, taking up proportionally more space within the thoracic cavity. With the appearance of lungs at Gosner stage 43, the heart is pushed down to a more ventral position because the lungs come to lie between the bottom of the animal's mouth and its heart. This pattern becomes even more pronounced as the lungs grow larger up to

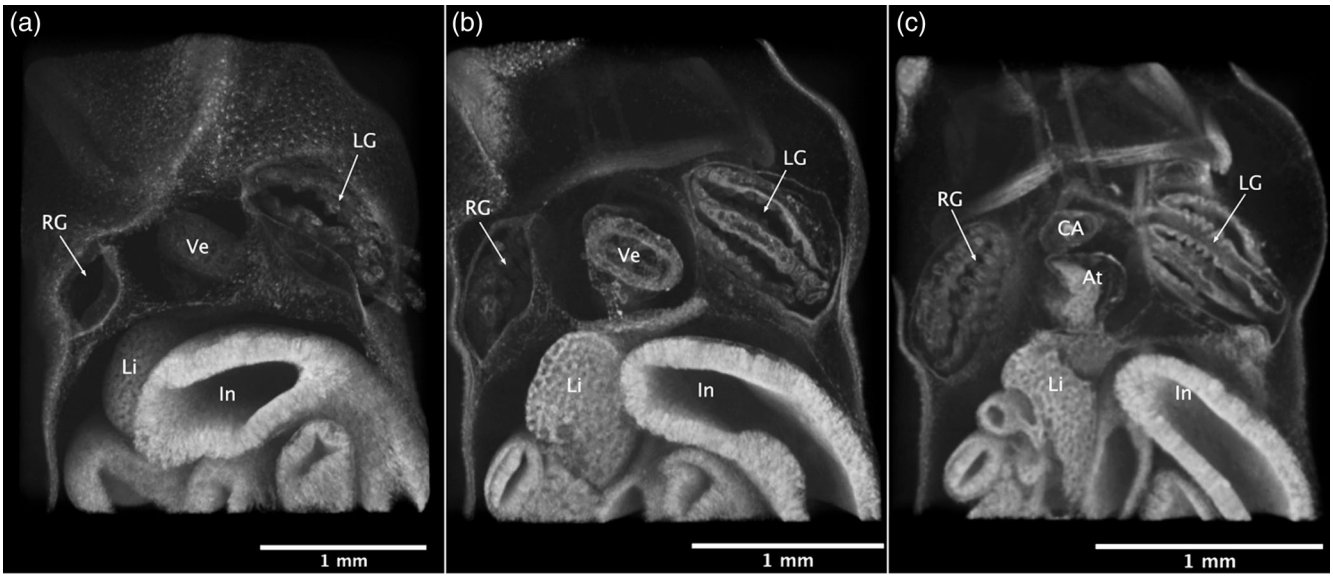

FIGURE 14 (a–c) Virtual horizontal cutaway of the ventral side of a *Bufo bufo* tadpole at Gosner stage 23 showing the asymmetry of the process of gill absorption and covering, and formation of the opercular spout. At, atrium; CA, conus arteriosus; In, intestines; LG, left gills; Li, liver; RG, right gills; Ve, ventricle

Gosner stage 46, when the larva has turned into a small froglet and metamorphosis is complete.

3.2 | Gills and aortic arches

No gills are present at Gosner stage 18, but the blood vessels originating from the area of the truncus arteriosus already extends into the general area where gills will soon develop.

At the transition from Gosner stage 18 to 19, the carotid arch starts to protrude into the outside, followed by the systemic and pulmocutaneous arches, forming what already resembles very small gills (see Figure 12a).

At the point of reaching Gosner stage 19, a small tuft of external gills is present. Already, each of the three aortic arches originating from the heart each reaches into its corresponding gill arch. The hyoid arches are forming a cover for this tuft of gills (see Figure 12b).

This situation remains the same up until Gosner stage 23 (see Figure 12b,c). Here, the hyoid gill cover starts to grow and soon contacts the animal's ventral side. While this skin folds continues to grow, it starts to cover the external gills, but it initially maintains a small opening on both sides out of which the gill tufts protrude (see Figure 13).

Soon, within the same Gosner stage, an asymmetric pattern within the development of internal gills starts to appear. The skin fold continues growing over the right gill toward its ventral side while only the right gill tufts start to withdraw and become shorter, so that they become fully covered by this skin fold. On the left side

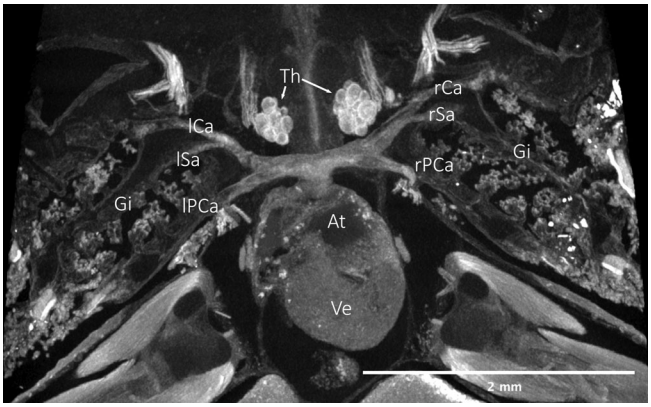

FIGURE 15 Gills and aortic arches of a *Bufo bufo* tadpole at Gosner stage 43, almost at the end of metamorphosis. Dorsal view of a virtual cutaway. A small lung sack is already in place (not visible here). However, aortic arches still lead directly into the gills. At, atrium; Gi, gills; lCa, left carotid arch; lPa, left pulmocutaneus arch; lSa, left systemic arch; rCa, right carotid arch; rPCa, right pulmocutaneus arch; rSa, right systemic arch; Th, thyroid glands; Ve, ventricle

however, the opening remains and the gill tuft continues to protrude. The left gill tuft eventually does withdraw into the gill cavity as well, and the remaining opening of the skin fold becomes smaller. This opening does not close completely as long as the metamorphosing animal still relies on gills for respiration but remains as the animal's opercular spout starting from Gosner stage 25 (see Figure 14).

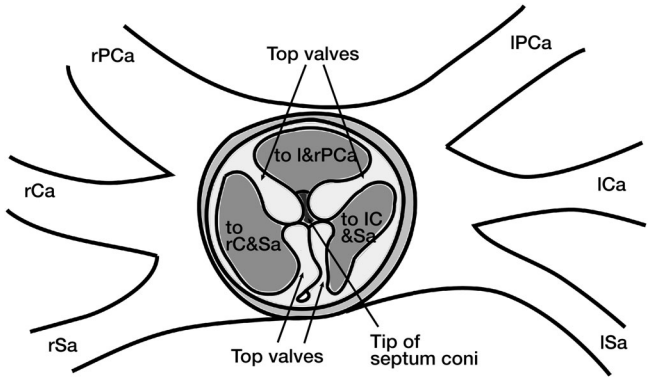

FIGURE 16 Schematic drawing of the conus arteriosus of *Bufo bufo* as suggested by the tadpole morphology at Gosner stage 29 in rostral view. The Y-shaped separation forming the three openings at the top of the conus is formed by the two top valves, each consisting of two separated leaflets that contact the tip of the septum coni protruding into the middle of this opening. lCa, left carotid arch; lPa, left pulmocutaneus arch; lSa, left systemic arch; rCa, right carotid arch; rPCa, right pulmocutaneus arch; rSa, right systemic arch

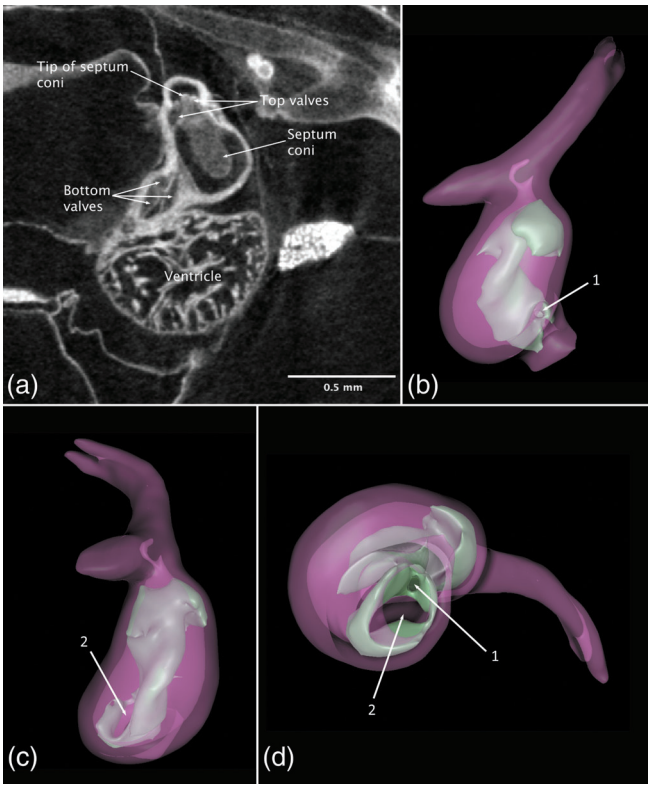

FIGURE 17 (a) Virtual micro-CT section through the heart of a PTA stained *Bufo bufo* tadpole at Gosner stage 40 showing the bottom valves, which form two openings into the conus at the ventricular-conal junction. The valves can be understood as either three separate ones or two main ones with one of them having an extra leaflet. Additionally, the septum coni and its tip reaching between the top valves are shown. (b, c) Segmentations of the conus arteriosus of an IKI stained *B. bufo* tadpole at Gosner stage 44 showing the two openings into the conus at the ventricular-conal junction (purple: conus wall, green: conal structures). (b) Lateral view of the side of the conus closer to the atrio-ventricular junction (left) showing how the small opening (1) aligns with the cavum pulmocutaneum. (c) Lateral view of the side of the conus further away from the atrio-ventricular junction (right) showing how the bigger opening (2) aligns with the cavum aorticum. (d) View through the transverse plane at the ventricular-conal junction showing the small (1) and big (2) opening into the conus. Note how the valvular tissue separating the two openings aligns with the septum coni. The rotating segmentations can be seen in Video 5 (conus_stage44)

Once the gills are situated fully within the now formed gill chambers, they become more finely branched, potentially facilitating gas exchange. This pattern continues up until metamorphic climax (see Figure 15). Only at Gosner stage 46, once the animal is already a small froglet, the gills start to recede very rapidly and are completely gone at the end of what is considered larval development.

4 | DISCUSSION

By taking into account a range of developmental stages and by using 3D micro-CT imaging, we were able to make a more detailed and comprehensive description of the conus arteriosus of *B. bufo* than has been previously available. Our results show that the finished conus has two major valves and a small extra leaflet at its junction with the ventricle, as well as two valves at the top with two small leaflets each, which, together with an upward-protrusion of the septum coni, form a Y-pattern (see Figures 11d–f and 16).

Furthermore, we found a small extra opening at the junction between the ventricle and the conus, separate from the large one that is surrounded by the row of valves (see Figure 17). Previously, de Graaf (1957) showed for *X. laevis* that the septum coni divides the conus into two chambers, the cavum aorticum that lies more ventrally and is in contact with the main orifice at the junction between ventricle and conus, and the cavum pulmocutaneum lying more dorsally (see Figure 11d–f). However, de Graaf also mentioned that it looks like the cavum pulmocutaneum has no direct communication with the ventricle, while also pointing out that this absence seems unlikely. We were able to find such a postulated opening for *B. bufo* in all specimens starting with Gosner stage 23 connecting the cavum pulmocutaneum with the ventricle. However, it is a rather small and narrow gap lying caudal to the main orifice, making it easy to miss when relying on histological sections alone—highlighting the need for 3D visualization in morphological research. In a short publication that was part of his estate, Hazelhoff (1952) had already shown such a small

extra opening on the left side of the ventricular-conal junction, which aligns with the cavum pulmocutaneum, in accordance with our results.

Following the two cava of the conus arteriosus up to the top rows of valves shows that they remain separated along the whole length of the conus by the spiraling of the septum coni (see Figure 6). Then, at the top of the conus, the upward protrusion of the septum and the two valves form three chambers. The two more rostral ones are in contact with the cavum aorticum and lead into the carotid and systemic aortic arches. The caudal-most opening is in contact with the cavum pulmocutaneum and leads into the pulmocutaneous aortic arch (see Figures 16 and 17).

Considering gross heart morphology, our results are in alignment with previous findings. Mohun et al. (2000) for example found a similar timing in heart compartmentalization in *X. laevis*. Additionally, the authors described the septum coni and atrial septum to be clearly resolved at Nieuwkoop-Faber (NF) stage 45/46 which would correspond to Gosner stage 25 in *B. bufo*, where said structures are already pronounced, even though we were able to show that they already start developing around Gosner stage 22. Atrial septation was found to be complete, and the left atrium is smaller than the right, as is typical for anurans (de Bakker, Wilkinson, & Jensen, 2015; Jensen, Wang, & Moorman, 2019).

The transition from external to internal gills during larval development is another important aspect to unraveling the conundrum that is tadpole respiration. Our results show that the external gills of *B. bufo* form in association with blood vessels protruding from the truncus arteriosus and start to withdraw into what will become the gill chamber, owing to a skin fold that starts from the hyoid and carotid arches and grows toward the ventral side and finally fully covers the right gills but leaves open a small opercular spout on the animal's left side (see Figures 13 and 14), which remains unchanged up to metamorphic climax.

This study offers a detailed description of the 3D morphology of a representative anuran conus arteriosus throughout larval development, as well as a description of gill development in *B. bufo*. The complete 3D image data are provided online in the Zenodo repository and can be used in future research on amphibian circulatory development and function.

ACKNOWLEDGMENTS

The authors are grateful to Dr. Silke Schweiger and Georg Gasser (NHM Vienna) for providing specimens and for helpful advice and discussions, and to Prof. Mihaela Pavlicev and the Theoretical Biology Unit and Department of Evolutionary Biology for supporting this project as part of N.K.'s master's work.

CONFLICT OF INTEREST

The authors declare no conflicts of interest.

AUTHOR CONTRIBUTIONS

Nina Kraus: Conceptualization (lead); formal analysis (equal); investigation (equal); methodology (supporting); project administration (supporting); visualization (lead); writing – original draft (lead); writing – review and editing (supporting). **Brian Metscher:** Data curation (equal); investigation (equal); methodology (equal); project administration (lead); supervision (lead); visualization (supporting); writing – original draft (supporting); writing – review and editing (lead).

ETHICS APPROVAL STATEMENT

All applicable international guidelines were followed. Only museum specimens were used in this research.

VIDEO LEGEND FOR LINKED VIDEOS

VIDEO 1: (cutaway_whole_heart_Bufo): Virtual cutaway of a PTA stained whole adult heart of *Bufo bufo* showing the gross morphology consisting of the aortic arches, atrium, conus arteriosus, truncus arteriosus and the ventricle.

VIDEO 2: (Bufo_conus_cutaway_sloweddown): Virtual cutaway of a PTA stained whole adult heart of *Bufo bufo*, showing the conus arteriosus and its internal structures in detail.

VIDEO 3: (stage_22_contour_mesh_conus): Rotating segmentations of the conus arteriosus of a *Bufo bufo* tadpole at Gosner stage 22. Red: conus wall. Pink: conal structures.

VIDEO 4: (stage_43_contour_mesh_conus): Rotating segmentations of the conus arteriosus of a *Bufo bufo* tadpole at Gosner stage 43. Red: conus wall. Pink: conal structures.

VIDEO 5: (conus_stage44): Rotating segmentations of the conus arteriosus of a *Bufo bufo* tadpole at Gosner stage 44 emphasizing the bottom valves, which form two openings into the conus at the ventricular-conal junction. Purple: conus wall. Green: conal structures.

DATA AVAILABILITY STATEMENT

The illustrated image data will be archived in the Zenodo repository, doi:10.5281/zenodo.5052677.

ORCID

Nina Kraus https://orcid.org/0000-0002-6135-262X
Brian Metscher https://orcid.org/0000-0002-6514-4406

REFERENCES

de Bakker, D. M., Wilkinson, M., & Jensen, B. (2015). Extreme variation in the atrial septation of caecilians (Amphibia: Gymnophiona). *Journal of Anatomy*, *226*, 1–12.

de Graaf, A. R. (1957). Investigations into the distribution of blood in the heart and aortic arches of *Xenopus laevis* (Daud.). *Journal of Experimental Biology*, *34*, 143.

Gosner, K. L. (1960). A simplified table for staging anuran embryos and larvae with notes on identification. *Herpetologica*, *16*, 183–190.

Hazelhoff, E. H. (1952). Die Trennung der Blutmassen mit verschiedenem Sauerstoffgehalt im Froschherzen. *Experientia*, *8*, 471–472.

Ison, R. E. (1967). The structure of the conus arteriosus of adult *Rana temporaria* L. (Amphibia). *Journal of Natural History*, *1*, 491–499.

Ison, R. E. (1968). The development of the heart of *Rana temporaria* L. *Journal of Natural History*, *2*, 449–457.

Jensen, B., van den Berg, G., van den Doel, R., Oostra, R.-J., Wang, T., & Moorman, A. F. M. (2013). Development of the hearts of lizards and snakes and perspectives to cardiac evolution. *PLoS One*, *8*, e63651.

Jensen, B., Wang, T., & Moorman, A. F. M. (2019). Evolution and development of the atrial septum. *Anatomical Record*, *302*, 32–48.

Johansen, K., & Hanson, D. (1968). Functional anatomy of the hearts of lungfishes and amphibians. *American Zoologist*, *8*, 191–210.

Kardong, K. V. (2009). *Vertebrates: Comparative anatomy, function, evolution*. Boston, MA: McGraw-Hill Higher Education.

Kolker, S. J., Tajchman, U., & Weeks, D. L. (2000). Confocal imaging of early heart development in *Xenopus laevis*. *Developmental Biology*, *218*, 64–73.

Mercola, M., Guzzo, R. M., & Foley, A. C. (2010). Chapter 1.3 - Cardiac development in the frog. In N. Rosenthal & R. P. Harvey (Eds.), *Heart development and regeneration* (pp. 87–102). Boston, MA: Academic Press.

Metscher, B. D. (2009). MicroCT for developmental biology: A versatile tool for high-contrast 3D imaging at histological resolutions. *Developmental Dynamics*, *238*, 632–640.

Metscher, B. D. (2011). X-ray microtomographic imaging of intact vertebrate embryos. *Cold Spring Harbor Protocols*, *2011*, 1462–1471.

Mohun, T. J., Leong, L. M., Weninger, W. J., & Sparrow, D. B. (2000). The morphology of heart development in *Xenopus laevis*. *Developmental Biology*, *218*, 74–88.

Mutterer, J., & Zinck, E. (2013). Quick-and-clean article figures with FigureJ. *Journal of Microscopy*, *252*, 89–91.

Rugh, R. (1951). *The frog: Its reproduction and development*. Philadelphia and Toronto: The Blakiston Company.

Schindelin, J., Arganda-Carreras, I., Frise, E., Kaynig, V., Longair, M., Pietzsch, T., ... Cardona, A. (2012). Fiji: An open-source platform for biological-image analysis. *Nature Methods*, *9*, 676–682.

Sharma, H. L. (1961). The circulatory mechanism and anatomy of the heart of the frog, *Rana pipiens*. *Journal of Morphology*, *109*, 323–349.

Simons, J. R. (1957). The pulmonary return as an agent in the final development of the atrium in *Rana temporaria*. *Journal of Embryology and Experimental Morphology*, *5*, 250–255.

How to cite this article: Kraus, N., & Metscher, B. (2022). Anuran development: A reinvestigation of the conus arteriosus and gill formation in *Bufo bufo* throughout metamorphosis using micro-CT. *The Anatomical Record*, *305*(5), 1100–1111. https://doi.org/10.1002/ar.24766